ADVANCED MATERIALS
www.advmat.de

Heat Engine Drives Transport of an $Fe^{II}_4L_4$ Cage and Cargo

*Bao-Nguyen T. Nguyen, Angela B. Grommet, Arnaud Tron, Maureen C. A. Georges, and Jonathan R. Nitschke**

The directed motion of species against a chemical potential gradient is a fundamental feature of living systems, underpinning processes that range from transport through cell membranes to neurotransmission. The development of artificial active cargo transport could enable new modes of chemical purification and pumping. Here, a heat engine is described that drives chemical cargo between liquid phases to generate a concentration gradient. The heat engine, composed of a functionalized $Fe^{II}_4L_4$ coordination cage, is grafted with oligoethylene glycol imidazolium chains. These chains undergo a conformational change upon heating, causing the cage and its cargo to reversibly transfer between aqueous and organic phases. Furthermore, sectional heating and cooling allow for the cage to traverse multiple phase boundaries, allowing for longer-distance transport than would be possible using a single pair of phases.

Complex polyhedral coordination cages are prepared from simple precursors through self-assembly,[1–15] whereby coordination bonds form and rearrange in seeking an energetic minimum.[16] The resulting lowest-energy structure often corresponds to a Platonic or Archimedean polyhedral solid.[5,16,17] These cages contain hollows that are capable of binding guest species.[6,8,14,18–23] Chemical stimuli, such as ions[2,24–27] or pH change,[12,28,29] can trigger the self-assembly process, manipulate the host–guest chemistry[12,25] of the complexes and modify their physical properties.[29] A temperature swing is among the most attractive stimuli, as it is easily reversible and leaves no chemical residue, in contrast with the addition of salts, acids, or bases. Thermal stimulation has been reported to trigger the reversible structural transformation of coordination complexes[30–32] and to open a switchable platinum-based molecular lock.[33]

Here, we report a thermoresponsive $Fe^{II}_4L_4$ coordination cage **1** (**Figure 1**), whose exterior is grafted with 12 pendant 1-methylimidazole PEG_{1000} ($PEG_{1000}(mim)^+$) chains. Heating and cooling led these $PEG_{1000}(mim)^+$ chains to expand and contract, respectively. These conformational changes were observed to modulate the solubility preference of cage **1** in the presence of an ionic liquid[34] (Figure 1), driving reversible phase transfer of the cage between water and ethyl acetate (EA). By alternating water and EA layers and controlling the thermal gradient along the length of a glass tube, thermoresponsive cage **1** was used to pump a molecular cargo, 1-fluoroadamantane (FA), directionally across the tube and back. By using thermal energy to accomplish work, i.e., the transportation of a cargo over a distance of 2 cm, this chemical system thus constitutes a novel class of heat engine, which is defined as a system that uses a temperature differential to perform work.[35,36]

The solubility preferences of cages rely on the affinities of their counterions for different solvent phases,[24,26] a phenomenon which can be used to effect phase transfer,[27,37] but which leads to an accumulation of salts in systems. In order to use other stimuli to drive phase transfer, the cage must be constructed such that the solvent preference of the counteranions does not predominate. To overcome this preference, we built upon the work of Yao et al.,[34] who demonstrated the phase transfer of the ionic liquid $[PEG_{1000}(mim)_2][NTf_2]_2$ (**IL**) between water and EA using heat as a stimulus. The hydrophobicity of the NTf_2^- anion of **IL** was outweighed by the solvent preference of the $PEG_{1000}(mim)_2^{2+}$ cation, allowing dissolution in either an aqueous or organic phase.

We hypothesized that $PEG_{1000}(mim)^+$ chains, appended to the vertices of coordination cages, would enable these cages to undergo thermally driven phase transfer despite their hydrophobic NTf_2^- counterions. Coordination cage **1** was thus prepared as the triflimide salt, $\mathbf{1}[NTf_2]_{20}$, from triamine **L1**[10](4 equiv.), $PEG_{1000}(mim)^+$-functionalized formylpyridine **L2** (12 equiv.), and iron(II) bis(trifluoromethanesulfonyl)imide ($Fe^{II}(NTf_2)_2$, 4 equiv.) in acetonitrile (Figure 1a). Subcomponents **L1** and **L2** reacted to form pyridylimine moieties that coordinated to four Fe^{II} centers at the cage vertices, with threefold-symmetric residues of **L1** capping each face of the tetrahedron. With three $PEG_{1000}(mim)^+$ chains at each cage vertex, twelve chains thus give rise to the thermal responsivity of the cage. At elevated temperatures, the PEG_{1000} chains expand, exposing hydrophobic ethylene groups and rendering the cage more soluble in EA and less soluble in water. Conversely, at lower temperatures, the PEG_{1000} chains coil,[34] facilitating hydrogen bonding between water and the exposed PEG ether oxygen atoms, and increasing the charge density of the cage. Its solvent preference is then reversed, rendering **1** soluble in water and insoluble in EA.

To investigate the conformational change experienced by cage **1** upon heating, a variable temperature (VT) ^{1}H DOSY

B.-N. T. Nguyen, Dr. A. B. Grommet, Dr. A. Tron, M. C. A. Georges, Prof. J. R. Nitschke
Department of Chemistry
University of Cambridge
Cambridge CB2 1EW, UK
E-mail: jrn34@cam.ac.uk

The ORCID identification number(s) for the author(s) of this article can be found under https://doi.org/10.1002/adma.201907241.

DOI: 10.1002/adma.201907241

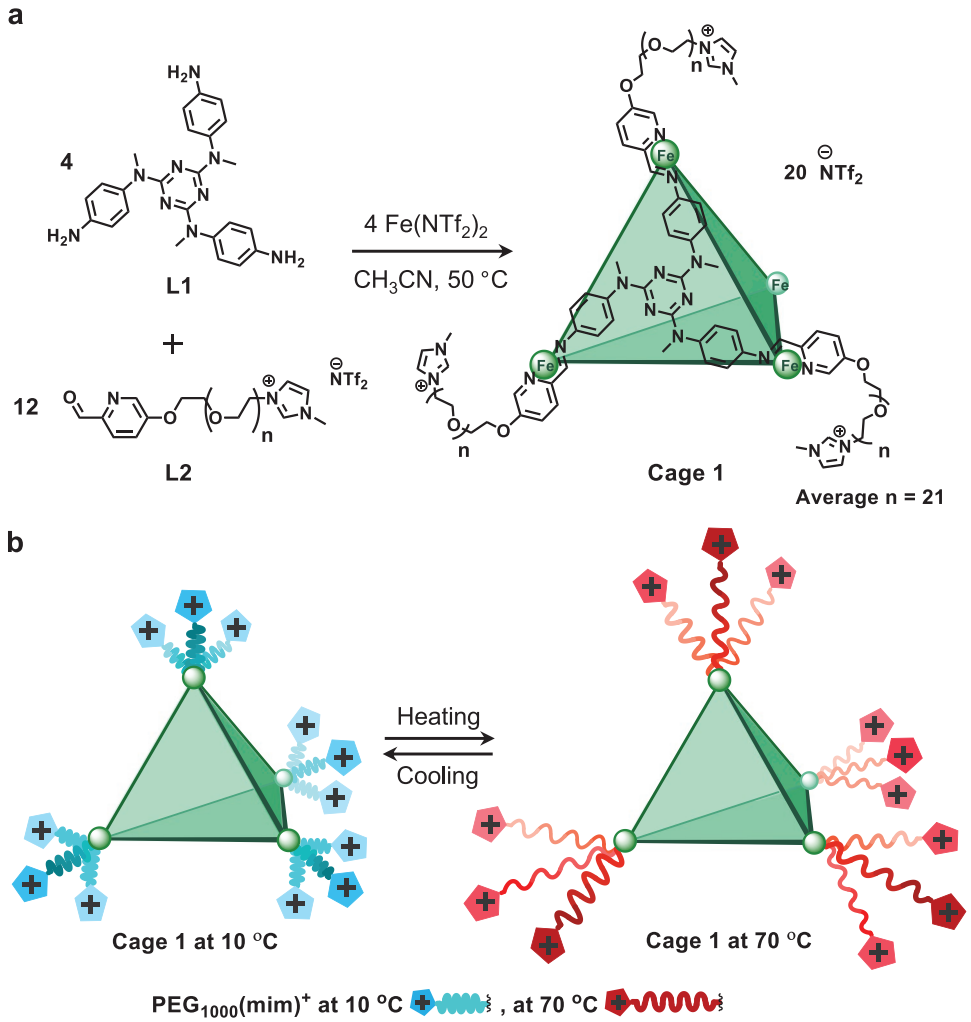

Figure 1. Synthesis and thermal responsivity of **1**. a) Cage **1** was prepared from the reaction of triamine (**L1**) and functionalized aldehyde (**L2**) subcomponents with $Fe^{II}(NTf_2)_2$. b) At 10 °C, the $PEG_{1000}(mim)^+$ chains at the cage corners contract, exposing the charged imidazole terminals and ether oxygen atoms and rendering **1** soluble in water. At 70 °C, the $PEG_{1000}(mim)^+$ chains expand to expose the more hydrophobic ethylene groups, rendering **1** insoluble in water and soluble in ethyl acetate (EA).

NMR experiment was conducted by monitoring **1** (0.5×10^{-3} M, CD_3CN) between 10 °C and 70 °C. These conditions were chosen to minimize aggregation of cage **1**, which would distort the diffusion results. Although cage **1** comprises a single entity, we observed that the imidazolium groups tethered to the cage consistently report a higher diffusion rate than the cage core. We attribute this effect to the additional degrees of freedom experienced by the imidazolium groups, due to the flexibility of the PEG_{1000} chains. The difference between the diffusion coefficients measured for the cage core and for the pendant imidazolium groups can thus be used to probe the conformation of the PEG_{1000} chains (Figure S3, Supporting Information). At low temperatures, the difference in the diffusion coefficients for the cage core and the imidazolium groups is small, suggesting that the PEG_{1000} chains are coiled and the imidazolium groups reside close to the cage core. Above 40 °C, the difference between the two diffusion coefficients increases sharply, suggesting that the PEG_{1000} chains expand, distancing the imidazolium groups from the cage core and allowing them to move independently.

We expected that conformational changes within the PEG_{1000} chains would result in aggregation of cage **1** in water at higher temperatures. Accordingly, the thermal responsivity of functionalized cage **1** was probed using variable temperature dynamic light scattering (VT DLS) (5 °C –35 °C) and VT UV–vis (5 °C –50 °C) to monitor a solution of cage **1** in water (1.7×10^{-3} M). DLS measurements (Figure S4, Supporting Information) indicate that aggregates of cage **1** exist even at low temperatures; from 5 °C to 30 °C, the diameter of these aggregates averages ≈100 nm. Upon heating to 35 °C, these aggregates increase in size to 450 nm in diameter. At 40 °C, the aggregates are no longer within the range of detection by DLS, but a significant increase in the baseline of the UV–vis spectrum (Figure S5a, Supporting Information) can be detected, suggesting that the size of these aggregates has grown further. At 50 °C, cage **1** can be observed separating out of aqueous solution (Figure S5b, Supporting Information). Significantly, the conformational changes observable by VT ^1H DOSY occurred within a similar temperature range as the aggregation of cage **1**, as observed by VT DLS and VT UV–vis. We therefore

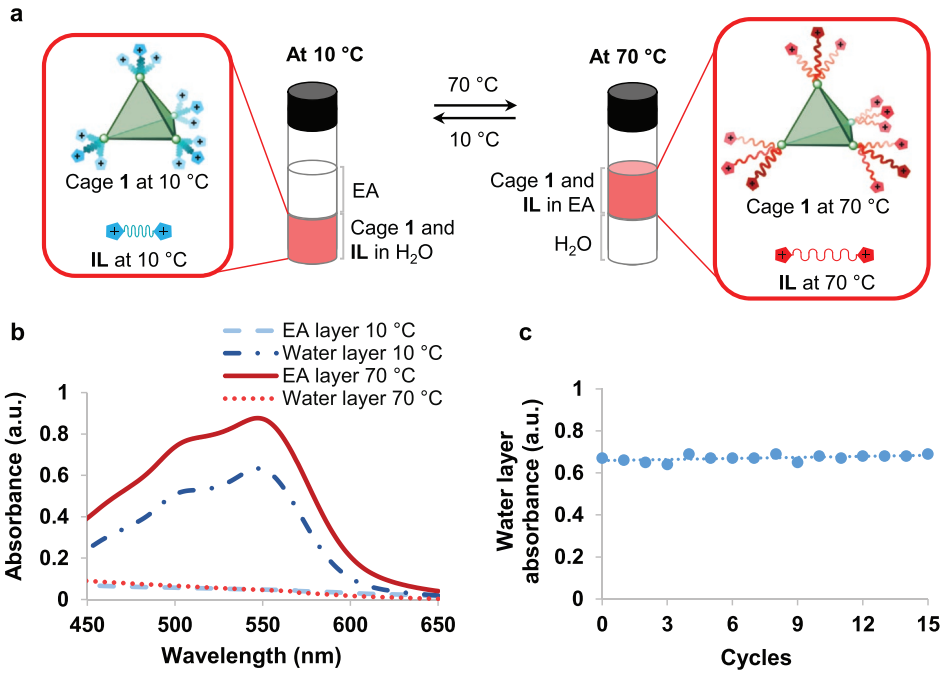

Figure 2. Phase transfer of cage **1** in a biphasic system. a) Cage **1** transferred between ethyl acetate (EA) and water phases upon heating and cooling. b) The UV–vis absorbance spectra of H_2O and EA layers in the biphasic system at 10 °C and 70 °C. At 10 °C, absorbance assigned to **1** (550 nm) was observed in the water layer while no absorption was seen in the EA layer. In contrast, at 70 °C, the EA layer showed absorption at 550 nm, assigned to **1**, whereas the water layer displayed no signal. c) Absorbance at 550 nm in the water layer at 10 °C was recorded over 15 cycles, over which the absorbance values of the cage remained constant.

concluded that conformational changes within the PEG_{1000} chains are associated with aggregation of cage **1**.

The phase transfer of cage **1** from water to EA and back again was monitored by UV–vis spectroscopy. At 10 °C, **1** (0.4×10^{-3} M) and **IL**[34] (87.2×10^{-3} M) were dissolved in water; a layer comprising an equal volume of EA was added, and the system was shaken to ensure thorough mixing of all components. A UV–vis spectrum was then recorded for each layer. In water at 10 °C, a strong absorbance was observed at 550 nm, attributed to the MLCT absorptions of **1** (Figure S1a, Supporting Information). No such absorption was observed in the EA layer, indicating that **1** resides exclusively in the water layer at low temperatures. When the system was heated to 70 °C, the cage was observed to transfer from the water layer to the EA layer within 30 s. A strong absorbance at 550 nm from **1** was thus observed in the EA layer, but no significant signal was detected in the water layer, indicating complete transport of **1** from water to the EA layer at 70 °C. Upon cooling to 10 °C, **1** transitioned back to the water layer within 30 s, as confirmed by UV–vis spectra of both layers (**Figure 2**b). A portion of EA layer was lost due to evaporation when the biphasic system was heated to 70 °C, just below the boiling point of EA (77 °C). As a result, the concentration of **1** and **IL** in the EA layer increased, leading to stronger absorbance of cage **1** in the EA layer. To investigate the efficiency of the phase transfer process, the transit of **1** back and forth between EA and water layers was followed over 15 cycles. The absorbance of **1** at 550 nm in the water layer following each cycle was recorded and observed to remain at a value of 0.67 ± 0.03, suggesting that the cage was stable to heating at 70 °C, and reflecting efficient phase transfer (Figure 2c).

To better understand the requirements of the phase transfer system, we undertook two control experiments. First, a solution of cage **1** (1.7×10^{-3} M) in water (0.2 mL) was prepared, and EA (0.2 mL) was added to create a biphasic system containing no **IL**. Cage **1** was soluble in water at room temperature, but failed to transport into EA upon heating to 70 °C (Figure S6a, Supporting Information). This experiment illustrated the critical role of **IL** in enabling the movement of the cage between layers. Second, we tested whether functionalization of the cage with $PEG_{1000}(mim)^+$ chains was necessary for phase transfer. The triflimide salt of the parent cage **2**, constructed using 2-formylpyridine in place of **L2**, **2**$[NTf_2]_8$, is insoluble in water, but the sulfate salt **2**$[SO_4]_4$[14] is water soluble. The addition of **IL** to either **2**$[NTf_2]_8$ or **2**$[SO_4]_4$ did not result in a material that underwent thermally switchable phase transfer (Figure S6b–d, Supporting Information). We infer that the triflimide counteranions paired with cationic **2**, giving **2**$[NTf_2]_8$, which is not rendered soluble in water by **IL**. Counterion solubility effects thus predominate in the absence of $PEG_{1000}(mim)^+$ chains grafted onto the cage framework, as expected based upon prior work.[7,10] Both additional **IL** and a functionalized cage framework thus appear necessary for thermoswitchable phase transfer to occur.

Having characterized the thermoswitchable phase transfer of cage **1** between water and EA, we then investigated the ability of the cage to transport molecular cargo between these two phases. The chosen test cargo was 1-fluoroadamantane (FA), which is known to bind strongly within **2**$[SO_4]_4$[26] in slow exchange on

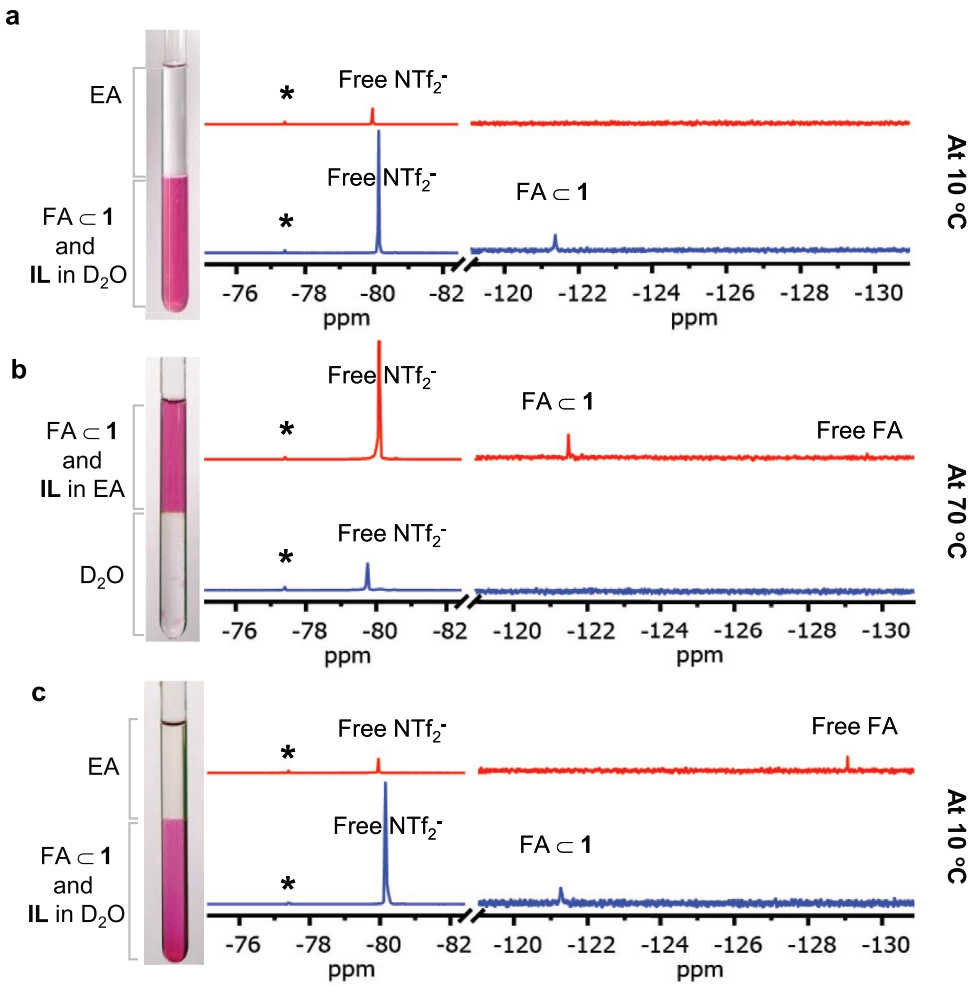

Figure 3. Following the phase transfer of **1** and its fluoroadamantane (FA) cargo in a biphasic system by ^{19}F NMR (471 MHz). a) ^{1}H NMR of the EA and D_2O layers. The strong NTf_2^- and encapsulated FA signals remained in the D_2O layer, indicating the presence of FA ⊂ **1** and **IL** in D_2O at 10 °C. b) At 70 °C, the majority of the NTf_2^- signal was observed in the EA layer, suggesting that **1** and **IL** had undergone phase transfer. The encapsulated FA signal observed in the EA layer affirmed cargo transport from the aqueous layer to the organic layer. c) When the system was cooled back to 10 °C, **1** and its cargo shuttled back to the D_2O layer, indicated by the strong signal corresponding to free NTf_2^- and the encapsulated FA peak in the water layer. The spectra were referenced to CF_3CH_2OH (20 mM) at –77.40 (marked as *).

the NMR timescale.[38] Because cage **2** shares the same framework as **1**, we anticipated that FA would behave similarly within the cavity of **1**.

Thermoswitchable transport of FA as a molecular cargo for cage **1** was investigated in a biphasic system of water and EA over a complete phase transfer cycle. FA ⊂ **1** (0.68 µmol) and **IL** (34.8 µmol) were initially loaded into the water layer (0.4 mL) at 25 °C. A layer of EA (0.4 mL) was added, and the sample was gently inverted to mix the two layers. The organic and aqueous layers were then separated, and ^{19}F NMR was used to analyze both layers. In the water layer, ^{19}F signals corresponding to FA ⊂ **1** and the triflimide anions from **1** and **IL** were observed at 121.4 and –80 ppm, respectively (**Figure 3**a). A triflimide signal was also observed in the EA layer, indicating the presence of a small amount of **IL**.

The layers were then recombined, and the temperature was increased to 70 °C, triggering the transport of FA ⊂ **1** from water into EA. The separated layers were again analyzed by NMR. The intensity of the ^{19}F signal from triflimide decreased in water and increased in EA, consistent with phase transfer of **IL** and FA ⊂ **1**. Furthermore, the ^{19}F signal attributed to encapsulated FA was observed only in the EA layer, leading us to infer transport of molecular cargo across the phase boundary; only a trace amount of free FA was also observed in the EA layer (–129 ppm, Figure 3b). The recombined layers were cooled to 10 °C and mixed gently, causing FA ⊂ **1** to transport back into the aqueous layer, as verified by ^{19}F NMR (Figure 3c).

To ensure that cage **1** was indeed the agent responsible for the transport of the molecular cargo FA between water and EA, we carried out a control experiment to test whether **IL** was capable of transporting FA in the absence of **1**. An aqueous solution of **IL** (87.2×10^{-3} M) was combined with an equal volume of FA solution (2×10^{-3} M) in EA to prepare a biphasic system comparable to the experiment employing **1**. Upon heating to 70 °C, **IL** was observed to transfer to the EA layer, which contained the FA. Upon cooling to 10 °C, **IL** was transferred back

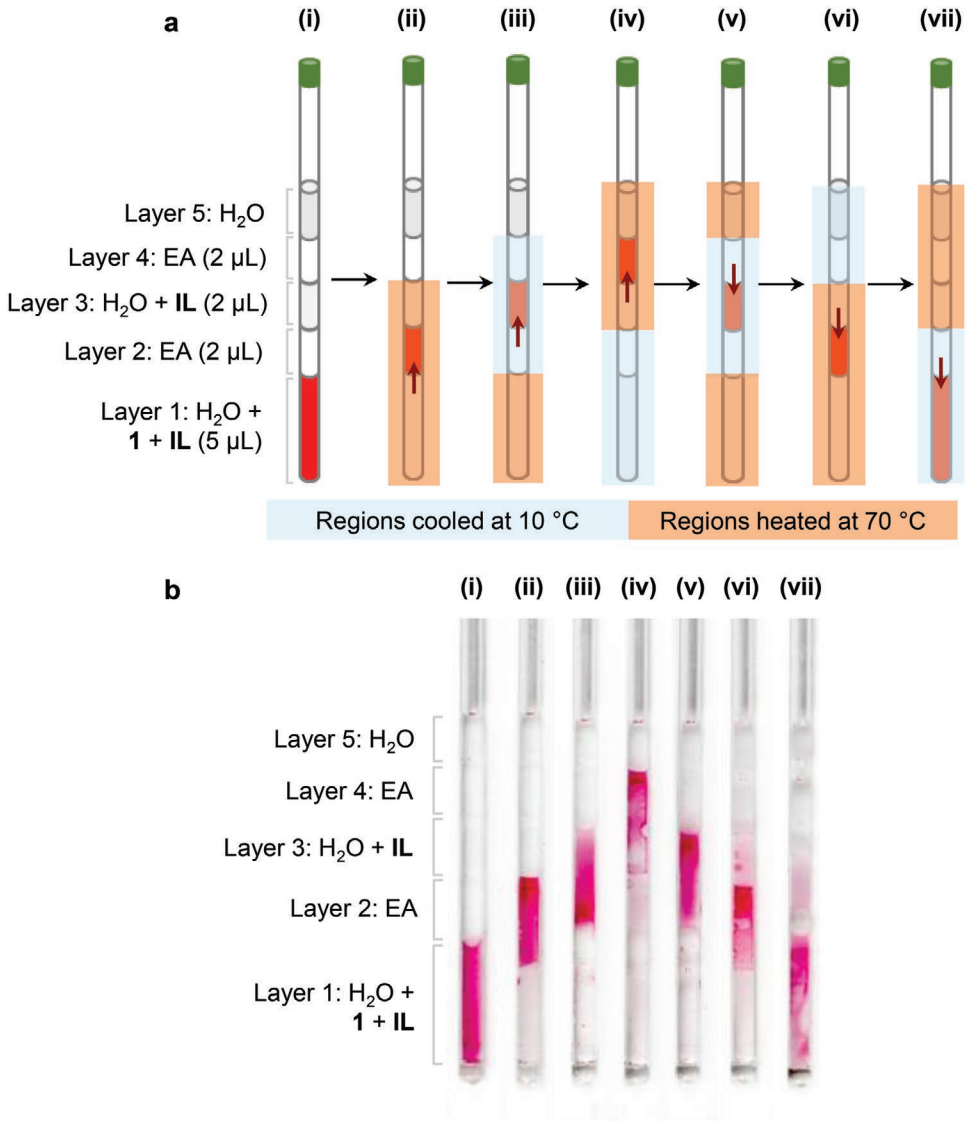

Figure 4. Cage **1** transfers between multiple phases upon sectional heating and cooling. a) Schematic illustration of a multiple layer system in a glass tube, with **1** (0.2×10^{-3} M) and **IL** (58×10^{-3} M) initially present in aqueous layer 1 (5 µL). Additional EA (2 µL) and aqueous (2 µL) layers were then added to create a four-phase system. Finally, a layer of water (2 µL) was added on top of EA layer 4 to prevent EA evaporation. Sectional heating (illustrated in orange) and cooling (blue) drove phase transfer of **IL** and **1** along the tube and back. b) Photographs were taken to record the phase transfer of **1** (red) at each of the corresponding stages.

to the water layer, with no FA signal observed in the water layer (Figure S10, Supporting Information). Transportation of FA thus occurred only within the cavity of cage **1**.

The thermoresponsive phase transfer concept described above was then developed into a four-phase system, with alternating aqueous and EA layers along the length of a glass tube (length: 35 mm, internal diameter: 1 mm). A final water layer was placed on top of layer 4 (EA) to prevent EA evaporation during the experiment. Cage **1** and **IL** were initially loaded into aqueous layer 1 and were subsequently transferred from layer to layer along the length of the tube and back again (**Figure 4**a). Layers 1 (aqueous), 2 (EA), and 3 (aqueous) were heated together to 70 °C, causing **1** to transfer from layer 1 to layer 2. Because the cage is insoluble in water at 70 °C, hot aqueous layer 3 acted as a barrier to prevent migration of the cage further along the tube (Figure 4a-ii), thus compartmentalizing cage **1** within EA layer 2.

In the next step, **1** and **IL** were transported to aqueous layer 3 by maintaining layer 1 at 70 °C, while simultaneously cooling layers 2, 3, and 4 to 10 °C. As **1** transfers selectively into water at low temperatures, transport from EA layer 2 could have resulted in movement from either aqueous layer 1 or 3. Because layer 1 was maintained at 70 °C, back transport was not observed of **1** into its original layer. Instead, cage **1** transferred selectively into aqueous layer 3. Chilling of EA layer 4 prevented cage dispersion into this layer, as **1** is insoluble in EA at lower temperatures (Figure 4a-iii).

Using this method of selectively heating and cooling the different regions along the capillary tube, we directed the movement of **1** along a total path length of 20 mm (Figure 4a),

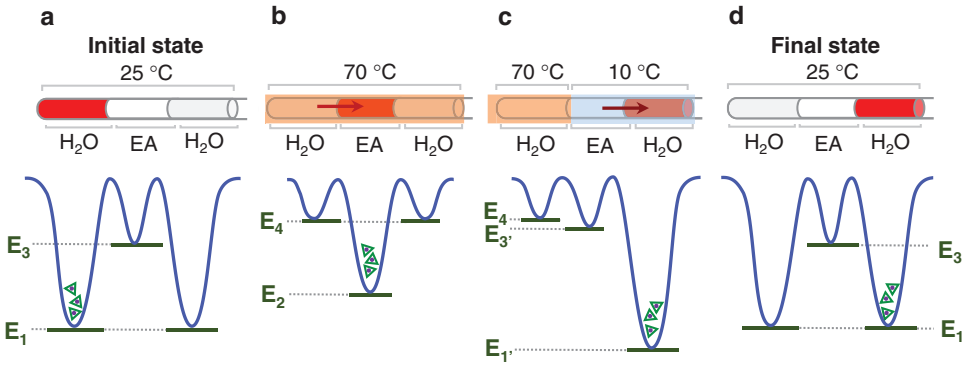

Figure 5. Energy diagrams showing the stepwise phase transfer process by which FA ⊂ **1** is driven out of equilibrium. a) In the initial state, FA ⊂ **1** was most soluble in water, as reflected in the accompanying energy diagram. b) Heating to 70 °C rearranged the energy levels such that FA ⊂ **1** became more stable in the EA layer. c) Cooling of the top two layers of the tube established a driving force for FA ⊂ **1** to undergo preferential phase transfer into the top water layer, in the "power stroke"[39,40] of the system. d) Upon return to room temperature, FA ⊂ **1** has become physically trapped in the upper water layer, out of equilibrium. E1 and E1′ are the energy levels of FA ⊂ **1** in water layers at 25 °C and 10°C, respectively, E3 and E3′ represent its energy levels in EA layers at 25 °C and 10 °C, respectively, and E2 and E4 are its energy levels in the EA and water layers, respectively, at 70 °C.

across six consecutive phase boundaries. UV–vis experiments (Figure 2) indicated that the location of **1** can be determined reliably based on the observation of its deep red color. The compartmentalization of **1** in alternating water and EA layers can thus been seen in photographs recorded at each stage in its movement along the tube (Figure 4b). As **1** and **IL** responded quickly to temperature changes, a portion of the material rapidly separated and accumulated near the phase boundaries as the tube was unwrapped in preparation for photography.

The small solution volume (2–5 µL) present in each layer of the four-phase system precluded monitoring of material transport using NMR experiments. To investigate the cargo transport ability of cage **1** in the four-phase system, a biphasic system containing EA (0.4 mL) and an aqueous layer containing FA ⊂ **1** (1.7×10^{-3} M, 0.4 mL) was set up. The system was subsequently heated and cooled in sequence, simulating the transport of FA ⊂ **1** into the EA layer and then back to the aqueous layer again. The cycle was repeated three times in total, matching the six phase-boundary crossings of FA ⊂ **1** in the four-phase system of Figure 4. Following these three cycles, ^{19}F NMR spectroscopy of the aqueous layer revealed that 71% of the FA cargo had been retained, consistent with effective cargo transport over multiple phase transitions (Figure S16, Supporting Information).

Figure 5 illustrates the functioning of our system as a heat engine, where **1** is pumped between the two lower aqueous phases shown in Figure 4. In the initial room-temperature state (a), FA ⊂ **1** prefers thermodynamically to reside in the initial aqueous phase. After the temperature was raised in b, the thermodynamics of the system shifted, bringing about phase transfer into the EA phase. Subsequent cooling of the top half of the tube (c) rearranged the energetic landscape so as to bring about directional transport of the cage into only one of the two aqueous phases. The process shown in c may be considered as the "power stroke" of the heat engine,[39,40] whereby the thermal gradient is translated into a chemical potential gradient, thus performing work. Following a return to room temperature (d), the cage population has been transferred to the top phase. The opening of a conduit between the upper and lower aqueous phases could in principle be used to capture a portion of the energy stored in the system in out-of-equilibrium state (d), provided that a thermodynamically unfavorable process could be coupled to the diffusion of cage through the conduit, so as to establish a uniform chemical potential at equilibrium.

From their initial development as power sources for the industrial revolution,[35] heat engines have been developed to encompass a range of mechanisms to translate the flow of heat into work.[35] Heat engines that establish a chemical potential gradient have even been postulated to play a role in the origins of life.[36,41] As many different cages have been reported based upon the pyridylimine ligand motif[42] of **1**, subcomponent **L2** may allow for the preparation of a diverse range of cages decorated with $PEG_{1000}(mim)^+$ chains. The sizes and shapes of these cages would define selectivity for the binding of many different guests, potentially allowing phase transfer systems based upon them to enable new methods of chemical purification.

Experimental Section

Synthesis of Subcomponent **L2**: A mixture of lithium bis(trifluoromethane)sulfonimide (1.5 equiv., 0.515 mmol, 148 mg) and $\mathbf{L2_d}$ (1 equiv., 0.343 mmol, 460 mg) in water (5 mL) was stirred for 2 h at room temperature. Dichloromethane (60 mL) was then added and the organic phase was washed with water (3 × 25 mL) and dried over $MgSO_4$. Dichloromethane was removed by rotary evaporation yielding subcomponent **L2** (480 mg, 97%) as a yellow oil. ^{1}H NMR (400 MHz, Methylene chloride-d$_2$) δ_H 9.95 (s, 1H, H_1), 8.91 (s, 1H, H_8), 8.46 (s, 1H, H_4), 7.93 (d, J = 8.7 Hz, 1H, H_2), 7.53 (d, 1H, H_{11}), 7.38 (d, 1H, H_{10}), 7.36 (d, 1H, J = 8.7 Hz, H_3), 4.37 (t, J = 4.6 Hz, 2H, H_d), 4.28 (t, J = 4.6 Hz, 2H, H_a), 3.95 (s, 3H, H_9), 3.88 (t, J = 4.6 Hz, 2H, H_b or H_c), 3.86 (t, J = 4.8 Hz, 2H, H_b or H_c), 3.67– 3.50 (m, 84H, $H_{aliphaticPEG}$). ^{13}C NMR (101 MHz, Methylene chloride-d2) δ_C 191.59 (C_1), 158.02 (C_7), 146.09 (C_5), 138.50 (C_4), 136.78 (C_8), 122.89 (C_{10} or C_{11}), 122.83 (C_{10} or C_{11}), 122.70 (C_2), 120.25 (C_3), 70.09 ($C_{aliphatic}$), 69.88 (C_a/C_b/C_c), 68.10 (C_a/C_b/C_c), 68.02 (C_a/C_b/C_c), 49.49 (C_d), 35.93(C_e). ^{19}F NMR (376.5 MHz, Acetonitrile-d$_3$) δ_F –79.52 (NTf_2^-).

Synthesis of Cage ***1***: Under nitrogen, 1,3,5-triazine-2,4,6-triamine, *N*,*N*′,*N*″-trimethyl-*tris*(4-aminophenyl) (**L1**) (4 equiv., 2.7 µmol, 1.2 mg), subcomponent **L2** (12 equiv., 7.88 µmol, 11.5 mg) and $Fe(NTf_2)_2{\cdot}4H_2O$ (4 equiv., 2.7 µmol, 1.7 mg) were added to degassed CD_3CN (400 µL).

The reaction mixture was heated to 50 °C for 18 h, affording a dark red solution of cage **1** (1.6×10^{-3} M). ^{1}H NMR (400 MHz, Acetonitrile-d_3) δ_H 8.70 (s, 12H, H_1), 8.59 (s, 12H, H_8), 8.43 (d, J = 9.0 Hz, 12H, H_2), 7.89 (d, J = 8.2 Hz, 12H, H_3), 7.44 (d, 12H, H_{11}), 7.37 (d, 12H, H_{10}), 7.35 (d, 12H, $H_{2'}$), 7.01 (s, 12H, H_4), 5.08 (d, 12H, $H_{3'}$), 4.27 (m, 48H, H_a&H_d), 3.84 (s, 36H, H_9), 3.79 (m, 48H, H_b&H_c), 3.54 (m, 1364H), 3.39 (s, 36H, $H_{1'}$). ^{13}C NMR (126 MHz, Acetonitrile-d_3) δ_C 172.93 (C_1), 164.43 ($C_{8'}$), 159.02 (C_5), 150.63 (C_6), 145.55 (C_4), 144.22 ($C_{7'}$), 136.7 (C_8), 131.63 (C_2), 124.95 ($C_{2'}$), 123.75 ($C_{4'}$), 123.24 (C_{10}), 122.85 (C_{11}), 122.65 (C_3), 121.20 ($C_{3'}$), 70.57 ($C_{aliphaticPEG}$), 68.25 (C_b & C_c), 49.59 (C_a & C_d), 37.11 ($C_{1'}$), 36.12 (C_9). ^{19}F NMR (376.5 MHz, Acetonitrile-d_3) δ_F -75.03 (encapsulated NTf_2^-), −80.09 (nonencapsulated NTf_2^-).

FA Transport by Cage **1** *in a Biphasic System*: In a vial, a biphasic system of ethyl acetate (EA) (0.4 mL) and water (0.4 mL), which contained fluoroadamantane in cage **1** (FA ⊂ **1**) (0.68 µmol) and **IL** (34.8 µmol), was set up. FA ⊂ **1** and **IL** transferred between the layers when the vial was heated to 70 °C in an oil bath or cooled to 10 °C in a cool water bath, followed by inversion to effect mixing of the layers. At each step of the phase transfer process, the EA and aqueous layers were separated, and NMR analysis was undertaken for each layer. The phases were recombined to reform the biphasic system for subsequent phase transfer steps.

Supporting Information

Supporting Information is available from the Wiley Online Library or from the author.

Acknowledgements

B.N.T.N. and A.B.G. contributed equally to this work. The authors thank Dr. Roy Lavendomme for NMR advice, Dr. Masahiro Yamashina for synthesis advice and Jack Hoffman for useful discussion about heat engines. This study was supported by the European Research Council (695009) and the UK Engineering and Physical Sciences Research Council (EPSRC, EP/P027067/1). B.N.T.N. acknowledges Agency of Science, Technology and Research (A-STAR) for PhD funding.

Conflict of Interest

The authors declare no conflict of interest.

Keywords

metal organic cages, molecular cargo transport, phase transfer, supramolecular chemistry, thermally responsive materials

Received: November 4, 2019
Revised: February 14, 2020
Published online:

[1] R. Freeman, M. Han, Z. Álvarez, J. A. Lewis, J. R. Wester, N. Stephanopoulos, M. T. McClendon, C. Lynsky, J. M. Godbe, H. Sangji, *Science* **2018**, *362*, 808.
[2] R. Zhu, J. Lübben, B. Dittrich, G. H. Clever, *Angew. Chem., Int. Ed.* **2015**, *54*, 2796.
[3] M. Yoshizawa, J. K. Klosterman, M. Fujita, *Angew. Chem., Int. Ed.* **2009**, *48*, 3418.
[4] G. H. Clever, P. Punt, *Acc. Chem. Res.* **2017**, *50*, 2233.
[5] F. J. Rizzuto, J. R. Nitschke, *Nat. Chem.* **2017**, *9*, 903.
[6] F. J. Rizzuto, L. K. S. Von Krbek, J. R. Nitschke, *Nat. Rev. Chem.* **2019**, *3*, 204.
[7] A. J. Mcconnell, C. J. E. Haynes, A. B. Grommet, C. M. Aitchison, J. Guilleme, S. Mikutis, J. R. Nitschke, *J. Am. Chem. Soc.* **2018**, *140*, 16952.
[8] G. H. Clever, M. Shionoya, *Chem. Eur. J.* **2010**, *16*, 11792.
[9] K. Harris, D. Fujita, M. Fujita, *Chem. Commun.* **2013**, *49*, 6703.
[10] J. L. Bolliger, T. K. Ronson, M. Ogawa, J. R. Nitschke, *J. Am. Chem. Soc.* **2014**, *136*, 14545.
[11] T. Asano, T. Okada, S. Shinkai, K. Shigematsu, Y. Kusano, O. Manabe, *J. Am. Chem. Soc.* **1981**, *103*, 5161.
[12] T. Tateishi, Y. Yasutake, T. Kojima, S. Takahashi, S. Hiraoka, *Commun. Chem.* **2019**, *2*, 25.
[13] X.-Z. Li, L.-P. Zhou, L.-L. Yan, Y.-M. Dong, Z.-L. Bai, X.-Q. Sun, J. Diwu, S. Wang, J.-C. Bünzli, Q.-F. Sun, *Nat. Commun.* **2018**, *9*, 547.
[14] Y. Liu, C. Hu, A. Comotti, M. D. Ward, *Science* **2011**, *333*, 436.
[15] M. Fujita, D. Oguro, M. Miyazawa, H. Oka, K. Yamaguchi, K. Ogura, *Nature* **1995**, *378*, 469.
[16] T. R. Cook, Y.-R. Zheng, P. J. Stang, *Chem. Rev.* **2013**, *113*, 734.
[17] K. Byrne, M. Zubair, N. Zhu, X.-P. Zhou, D. S. Fox, H. Zhang, B. Twamley, M. J. Lennox, T. Düren, W. Schmitt, *Nat. Commun.* **2017**, *8*, 15268.
[18] M. Yoshizawa, M. Tamura, M. Fujita, *Science* **2006**, *312*, 251.
[19] W. M. Bloch, Y. Abe, J. J. Holstein, C. M. Wandtke, B. Dittrich, G. H. Clever, *J. Am. Chem. Soc.* **2016**, *138*, 13750.
[20] G. Zhang, M. Mastalerz, *Chem. Soc. Rev.* **2014**, *43*, 1934.
[21] A. Galan, P. Ballester, *Chem. Soc. Rev.* **2016**, *45*, 1720.
[22] J. S. Mugridge, R. G. Bergman, K. N. Raymond, *J. Am. Chem. Soc.* **2011**, *133*, 11205.
[23] W. Cullen, M. C. Misuraca, C. A. Hunter, N. H. Williams, M. D. Ward, *Nat. Chem.* **2016**, *8*, 231.
[24] A. B. Grommet, J. B. Ho, E. G. Perca, D. J. Howe, J. L. Bolliger, J. R. Nitschke, *J. Am. Chem. Soc.* **2018**, *140*, 14770.
[25] S. Löffler, J. Lübben, L. Krause, D. Stalke, B. Dittrich, G. H. Clever, *J. Am. Chem. Soc.* **2015**, *137*, 1060.
[26] A. B. Grommet, J. R. Nitschke, *J. Am. Chem. Soc.* **2017**, *139*, 2176.
[27] D. Zhang, T. K. Ronson, J. Mosquera, A. Martinez, J. R. Nitschke, *Angew. Chem., Int. Ed.* **2018**, *57*, 3717.
[28] A. Ghosh, M. Haverick, K. Stump, X. Yang, M. F. Tweedle, J. E. Goldberger, *J. Am. Chem. Soc.* **2012**, *134*, 3647.
[29] A. Aggeli, M. Bell, L. M. Carrick, C. W. G. Fishwick, R. Harding, P. J. Mawer, S. E. Radford, A. E. Strong, N. Boden, *J. Am. Chem. Soc.* **2003**, *125*, 9619.
[30] Z.-Q. Yao, J. Xu, B. Zou, Z. Hu, K. Wang, Y.-J. Yuan, Y.-P. Chen, R. Feng, J.-B. Xiong, J. Hao, *Angew. Chem., Int. Ed.* **2019**, *58*, 5614.
[31] V. K. Rao, D. Miyajima, A. Nihonyanagi, T. Aida, *Nat. Chem.* **2017**, *9*, 1133.
[32] Y. Tu, F. Peng, X. Sui, Y. Men, P. B. White, J. C. M. Van Hest, D. A. Wilson, *Nat. Chem.* **2017**, *9*, 480.
[33] F. Ibukuro, T. Kusukawa, M. Fujita, *J. Am. Chem. Soc.* **1998**, *120*, 8561.
[34] W. Yao, H. Wang, G. Cui, Z. Li, A. Zhu, S. Zhang, J. Wang, *Angew. Chem., Int. Ed.* **2016**, *55*, 7934.
[35] K. E. Dorfman, D. V Voronine, S. Mukamel, M. O. Scully, G. R. Fleming, *Proc. Natl. Acad. Sci. USA* **2013**, *110*, 2746.
[36] W. J. A. Muller, D. Schulze-Makuch, *Phys. A* **2006**, *362*, 369.
[37] N. Mihara, T. K. Ronson, J. Nitschke, *Angew. Chem.* **2019**, *131*, 12627.
[38] A. B. Grommet, J. L. Bolliger, C. Browne, J. R. Nitschke, *Angew. Chem., Int. Ed.* **2015**, *54*, 15100.
[39] J. Chen, *J. Phys. D: Appl. Phys.* **1994**, *27*, 1144.
[40] I. A. Martínez, É. Roldán, L. Dinis, D. Petrov, J. M. R. Parrondo, R. A. Rica, *Nat. Phys.* **2016**, *12*, 67.
[41] W. J. A. Muller, *Prog. Biophys. Mol. Biol.* **1995**, *63*, 193.
[42] D. Zhang, T. K. Ronson, J. R. Nitschke, *Acc. Chem. Res.* **2018**, *51*, 2423.